

Pressure-dependent physical properties of cubic SrBO_3 (B=Cr, Fe) perovskites investigated by density functional theory

Md Zahid Hasan, Md Rasheduzzaman, and Khandaker Monower Hossain
Citation: Chin. Phys. B, 2020, 29 (**12**): 123101. DOI: 10.1088/1674-1056/abab7f
Journal homepage: http://cpb.iphy.ac.cn; http://iopscience.iop.org/cpb

What follows is a list of articles you may be interested in

Ab initio investigation of excited state dual hydrogen bonding interactions and proton transfer mechanism for novel oxazoline compound

Yu-Sheng Wang(王玉生), Min Jia(贾敏), Qiao-Li Zhang(张巧丽), Xiao-Yan Song(宋晓燕), Da-Peng Yang(杨大鹏)
Chin. Phys. B, 2019, 28 (**10**): 103105. DOI: 10.1088/1674-1056/ab4042

Theoretical insights into photochemical ESITP process for novel DMP-HBT-py compound

Guang Yang(杨光), Kaifeng Chen(陈凯锋), Gang Wang(王岗), Dapeng Yang(杨大鹏)
Chin. Phys. B, 2020, 29 (**10**): 103103. DOI: 10.1088/1674-1056/aba9bb

Density functional theory study of structural stability for gas hydrate

Ping Guo(郭平), Yi-Long Qiu(邱奕龙), Long-Long Li(李龙龙), Qiang Luo(罗强), Jian-Fei Zhao(赵建飞), Yi-Kun Pan(潘意坤)
Chin. Phys. B, 2018, 27 (**4**): 043103. DOI: 10.1088/1674-1056/27/4/043103

Ab-initio calculations of structural, electronic, and optical properties of $Zn_3(VO_4)_2$

Nisar Ahmed, S Mukhtar, Wei Gao, Syed Zafar Ilyas
Chin. Phys. B, 2018, 27 (**3**): 033101. DOI: 10.1088/1674-1056/27/3/033101

Excited state intramolecular proton transfer mechanism of o-hydroxynaphthyl phenanthroimidazole

Shuang Liu(刘爽), Yan-Zhen Ma(马艳珍), Yun-Fan Yang(杨云帆), Song-Song Liu(刘松松), Yong-Qing Li(李永庆), Yu-Zhi Song(宋玉志)
Chin. Phys. B, 2018, 27 (**2**): 023103. DOI: 10.1088/1674-1056/27/2/023103

Pressure-dependent physical properties of cubic $SrBO_3$ (B = Cr, Fe) perovskites investigated by density functional theory*

Md Zahid Hasan[1], Md Rasheduzzaman[1], and Khandaker Monower Hossain[2,†]

[1] Department of Electrical and Electronic Engineering, International Islamic University Chittagong, Kumira, Chittagong-4318, Bangladesh
[2] Department of Materials Science and Engineering, University of Rajshahi, Rajshahi-6205, Bangladesh

(Received 28 May 2020; revised manuscript received 6 July 2020; accepted manuscript online 1 August 2020)

We perform the first-principles investigations of the structural, elastic, electronic, and optical properties of $SrBO_3$ (B = Cr, Fe) perovskites under pressure based on density functional theory (DFT). This is the first detailed pressure-dependent study of the physical properties for these compounds. The calculated structural parameters are consistent with the existing experimental results and slightly decrease with the application of pressure. The mechanical properties are discussed in detail and reveal that the $SrCrO_3$ is harder than $SrFeO_3$. Without pressure, these compounds behave like half-metals, confirmed by their band structure and density of states. Although the $SrCrO_3$ retains its half-metallic nature under pressure, $SrFeO_3$ becomes metallic for both up-spin and down-spin configuration. Both charge density and bond overlap population reveal the covalent nature of Cr–O bond and Fe–O bond in the studied compounds. The optical properties of $SrBO_3$, also discussed for the first time, reveal some interesting results.

Keywords: density functional theory (DFT), effects of pressure, electronic band structure, optical properties

PACS: 31.15.E–, 62.20.–x, 71.20.–b, 78.20.Ci **DOI:** 10.1088/1674-1056/abab7f

1. Introduction

Recently, perovskite oxide (chemical formula ABO_3) has received significant attention from scientific researchers theoretically[1–6] and experimentally,[7–9] due to its phase transformation and significant applications in advanced technology. Owing to their unique physical properties such as ferroelectricity, piezoelectricity, high-temperature superconductivity, colossal magnetoresistivity, and ionic conductivity, the perovskite materials are highly important for numerous technological applications.[10–12] For example, researchers have demonstrated several improvements in spintronic and magneto devices.[13,14] Moreover, this type of oxideis exceptionally useful in solid-state fuel cells, gas separation membranes, high-temperature superconductors (HTSCs), optoelectronic devices, magneto–electronic and magneto–optic technologies, high-capacity memory, random-access memory, sensors, laser frequency doubling, host crystals, non-volatile memory, high k capacitors, and chemical reactors.[10,12,15–21] Usually, ABO_3 perovskites are crystallized into a cubic structure, where cation A is placed at the corner, cation B is a transition metal located in the center, and oxygen atom is located in the face-center of the unit cell.[3] It is evident that when cation B is replaced with a magnetic element (*e.g.*, Cr, Fe, *etc.*), the perovskite material will gain magneto–electric and multiferroic properties.[22–24] Perovskite material with d or f orbital in its electronic configuration possesses unprecedented physical properties.[25] In the exploration of perovskite oxides, $SrBO_3$ (B = Cr, Fe) has been reported elsewhere,[26,27] and crystallizes into a cubic perovskite structure with the space group *Pm-3m*. Zhou *et al.*[28] thoroughly investigated the structural features, magnetic susceptibility, and thermal and electrical conductivities of $SrCrO_3$. However, the differences in both the electronic (metal–semiconductor) and magnetic (Pauli paramagnetic Curie–Weiss behavior) properties studied by various researchers remain unexplained.[26,29–32] The metallic characteristic of $SrCrO_3$ was also reported in an earlier investigation based on the linear muffin-tin orbitals (LMTO) method.[33] On the other hand, cubic $SrFeO_3$ has a Fe^{4+} state, that exhibits metallic conductivity at 0.1 MPa and exhibited no phase transformation up to 74 GPa.[34–37] Saburo Nasu *et al.* elucidated the persistence of pressure-induced ferromagnetism (FM) in $SrFeO_3$.[35] In addition, a strong metallic bond was observed in the $SrFeO_3$ because of the robust interaction between 3d (Fe^{4+}) and 2p (O) electrons.[38] Moreover, the $SrFeO_3$ exhibited metallic conductivity, and the valence state of Fe remained constant below 4.2 K.[38,39] The transformation of phase from helical spin to FM at 7 GPa has also been observed.[40]

In recent years, the first-principles method has become the most striking theoretical approach to the investigation of the physical and chemical properties of solid materials. In the approach only atomic lattice constants are used as input parameters to solve the Schrödinger equation. Recently, in several theoretical studies on perovskite materials including AMO_3 (A = Pb, Ba, Sr, Ca),[41,42] $BaMO_3$ (M = Pr, Th, U),[43] $SnTaO_3$,[12] $SrTbO_3$,[17] ACO_3 (A = Ca, Sr),[16] and $SrHfO_3$[44] the first-principles calculations were conducted.

*Project supported by the Science Fund from the Ministry of National Science and Technology (NST), Bangladesh.
†Corresponding author. E-mail: monower37@gmail.com
© 2020 Chinese Physical Society and IOP Publishing Ltd

Moreover, in a few theoretical reports[45,46] on $SrCrO_3$ and $SrFeO_3$, and especially on $SrFeO_3$ and its derivatives,[47,48] density functional theory (DFT) calculations were performed. However, no pressure-dependent study regarding these two perovskites is yet available in the existing literature. Since pressure plays a significant role in determining material properties, it is necessary to further investigate these materials' behaviors under pressure. The pressure dependence of $SrBO_3$ (B = Cr, Fe) perovskites can yield a wealth of information regarding the structure, lattice dynamics, and electronic band structure related to the metallic conductivity. This is the main motivation for choosing these perovskites in the present study to investigate their structural stabilities and changes in physical properties under pressure. We employ the DFT-based Cambridge Serial Total Energy Package (CASTEP) to calculate and explore the pressure-dependent significant physical properties of $SrBO_3$ (B = Cr, Fe) for the first time to precisely understand these material systems and identify their potential applications. In this study, we investigate the materials' mechanical and elastic stabilities under pressure, which measures their suitability for device fabrication and other applications. At the same time, we also address the significant effects of pressure on their electronic properties. Moreover, the in-depth optical analyses of both systems provide information about their interactions with incident photons, which is very effective for optoelectronic and dielectric applications.

2. Computational method

The most commonly applied process for *ab-initio* modeling of structural, electronic, and optical properties of crystalline materials is DFT with periodic ambient condition. In this method, the ground state of the compound is established by resolving the Khon–Sham equation.[49] The choice of the exchange–correlations potential is quite important for reliably predicting the ground-state physical characteristics of the system. For metallic systems with weak electronic corrections, the generalized gradient approximation (GGA) tends to relax the crystal lattice and slightly overestimate the lattice constants. In this study, we adopt the GGA with the Perdew–Burke–Ernzerhof (PBE) functional[50] within CASTEP.[51] According to this plan, the comparatively improved level computation method GGA + U was adopted for all the property calculations (except mechanical properties where GGA is used), with spin polarized and formal spin used as the primary conditions. This particular function is well known for its general applicability and gives rather accurate results for the diverse classes of crystalline solids. We have also used Vanderbilt-type ultrasoft pseudopotential to account for the electron–ion interactions.[52] The Broyden–Fletcher–Goldfarb–Shanno (BFGS) geometry optimization[53] technique was used to optimize the crystal structure ($Pm\bar{3}m$, space group No. 221). The following electronic states were considered for the band structure calculations: Sr [$5s^2$], Cr [$3d^5 4s^1$], Fe [$3d^6 4s^2$], O [$2s^2 2p^4$]. The total energy of the cell volume was calculated by using the periodic Bloch boundary conditions. The tolerance levels for computations were set so that a very high level of convergence was achieved. An energy cutoff of 900 eV was used to expand the plane-wave basis set k-point sampling within the first Brillouin zone (BZ) following the Monkhorst–Pack grid scheme.[54] For precise K-space integration, $12 \times 12 \times 12$ K-point grids were used for our present calculations. The tolerance levels for computational convergence were set to be ultra-fine. The total energy 5×10^{-6} eV/atom, maximum force 0.01 eV/Å, maximum stress 0.02 GPa, and maximum ionic displacement 5×10^{-4} Å provided the optimum convergence tolerance for these calculations.

3. Results and discussion

3.1. Structural properties

First, the structures of $SrBO_3$ materials are constructed by using the experimentally reported crystallographic refinement results.[26,27] The $SrBO_3$ oxides each have a cubic perovskite (space group $Pm\bar{3}m$) crystal structure in which Sr holds the body center, B (= Cr, Fe) are at the corners, and O is located in the cube center. After geometry optimization, the structures of $SrBO_3$ are entirely relaxed. The optimized crystal structures of $SrCrO_3$ and $SrFeO_3$ as a structural model of the cubic $SrBO_3$ system are depicted in Fig. 1. The optimized lattice constants and cell volumes under different pressures are shown in Table 1. Ambient condition and theoretical and experimental results are also given for $SrCrO_3$ and $SrFeO_3$ when available (Table 1). The optimized structural parameters under ambient condition accord with previous experimental[26,27] and some theoretical results[45–48] of both perovskites under this study. As shown in Table 1, the values of lattice constants decrease with applied pressure increasing from 5 GPa to 10 GPa to 15 GPa to 20 GPa, reflecting the common tendency of crystalline materials.

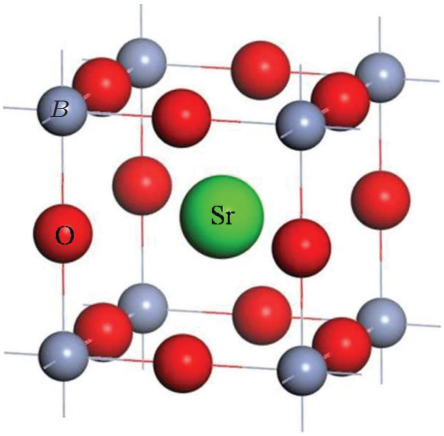


Fig. 1. Conventional crystal structure of $SrBO_3$ (B = Cr, Fe).

Table 1. Optimized structural parameters of SrBO_3 at different pressures.

Pressure/GPa	Compound	Lattice constant a/Å	Volume V/Å^3	Reference
0	$SrCrO_3$	3.897	59.197	this work
5		3.855	57.302	
10		3.819	55.717	
15		3.787	54.336	
20		3.759	53.127	
6		3.81765	–	Expt.[26]
8		3.81772	–	
10		3.81742	–	
0		3.756	–	Theor.[45]
0		3.85	–	Theor.[46]
0	$SrFeO_3$	3.922	60.343	this work
5		3.874	58.174	
10		3.831	56.229	
15		3.794	54.644	
20		3.759	53.140	
0		3.870	–	Expt.[27]
0		3.851	–	Theor.[47]
0		3.851	–	Theor.[48]

3.2. Mechanical properties

Various elastic properties of a crystal can reflect interatomic interactions and are very useful for understanding different solid-state properties under equilibrium condition. These include, among others, the solid's mechanical stability, bonding nature, machinability, and elasticity–plasticity.[55] In the case of cubic crystals, it is only necessary to calculate the three distinct elastic constants, *i.e.*, C_{11}, C_{12}, and C_{44} because for cubic symmetry, $C_{11} = C_{22} = C_{33}$, $C_{12} = C_{23} = C_{13}$, and $C_{44} = C_{55} = C_{66}$.[56] All the elastic constants are calculated through the finite strain theory using CASTEP[57] (Table 2).

Table 2. Calculated values of elastic constant (C_{ij} in unit GPa) of SrBO_3 at different pressures.

Pressure/GPa	Compound	C_{11}	C_{12}	C_{44}
0	$SrCrO_3$	242.295	135.310	114.707
5		270.733	141.999	120.904
10		307.949	158.570	126.669
15		344.981	174.959	132.134
20		374.727	184.386	137.255
0	$SrFeO_3$	144.876	150.184	108.396
5		181.933	172.977	111.938
10		211.310	187.668	121.140
15		241.382	203.500	128.406
20		276.835	224.389	131.934

No theoretical data on the elastic properties of SrBO_3 under increasing pressure are yet available. Therefore, no comparison can be made with other data for elastic properties. For ensuring mechanical stability, a material should gratify the Born–Huang stability criteria described by the following relations:[58]

$$C_{11} + 2C_{12} > 0, \quad C_{44} > 0, \quad C_{11} - C_{12} > 0. \tag{1}$$

The SrBO_3 satisfies the above criteria superbly at various pressures, affirming that it is mechanically stable under all pressure conditions (Table 2).

The knowledge of the elastic response of materials under various employed stress (pressure) is very useful in industrial applications that are governed by the C_{ij} of a single crystal. Among these, C_{11} is related to resistance to linear compression along the x direction, which increases with compression increasing. Note that the computed elastic constants are positive and increase as the pressure increases. The elastic constants meet all the stability criteria, indicating that the SrBO_3 is perfectly stable. Moreover, the calculated values of C_{11} for all perovskites are higher than C_{12}, except 0 GPa in $SrFeO_3$, which is a sign that the incompressibility along the crystallographic a axis is stiffer than along the b axis. Therefore, the bond along the [100] direction is harder than along the [011] direction. To understand the influence of pressure on molybdate, we investigate the elastic moduli, including bulk modulus B, shear modulus G, and Young modulus Y. These properties reveal the mechanical behaviors of solids, which can be estimated by using the Vigot–Reuss–Hill (VRH) approximation.[59] The VRH approximation is an average of two bonds, obtained by using the lower bound of Vigot and the upper bound of Reuss. This approximation is a prominent method to determine the mechanical features of solids for a single crystal with elastic constants.[60]

$$B = \frac{1}{2}(B_{\mathrm{V}} + B_{\mathrm{R}}), \quad G = \frac{1}{2}(G_{\mathrm{V}} + G_{\mathrm{R}}),$$
$$Y = \frac{9BG}{9B+G}, \qquad \nu = \frac{3B-2G}{3(3B+G)}. \tag{2}$$

The bulk modulus B, shear modulus G, and Young's modulus Y are indicative of stability against volume, shear, and longitudinal deformation and are closely related to the applied pressure on the solid. Table 3 shows that B, G, and Y of SrBO_3 at different pressures increase with pressure increasing. This is natural, since the applied pressure makes the crystal stiffer. The bulk modulus of $SrCrO_3$ in 0 GPa is compared with the theoretical data.[46] Otherwise, B, G, and Y of SrBO_3 are calculated for the first time at different pressures, *i.e.*, 5 GPa, 10 GPa, 15 GPa, and 20 GPa.

Pugh's and Poisson's ratios are very useful for accurately predicting the ductility, brittleness, and hardness of materials. According to the Pugh's ratio (B/G), and Poisson's ratio, all the pressure systems under study are ductile. Hardness tends to increase with pressure rising because the higher value of Pugh's and Poisson's ratios reflect the high hardness of the material and *vice versa*.[61,62] This increasing trend of hardness with the increase of pressure is very obvious. To confirm our

hardness prediction, we compute the Vickers hardness from the following equation:[55]

$$H_{\mathrm{V}} = \frac{(1-2\nu)Y}{6(1+\nu)}. \tag{3}$$

All the calculated values are listed in Table 3, and these values predict similar results to those suggested by Poisson's and Pugh's ratios. The hardness values for both compounds increase with increasing pressure, and it is seen that $SrCrO_3$ is harder than $SrFeO_3$. The cubic compounds $SrBO_3$ with ductile behaviors promise to be used in optoelectronic devices. The increasing trend of Poisson's ratio with pressure increasing indicates higher elasticity.[63]

Table 3. Estimated bulk modulus B (in unit GPa), shear modulus G (in unit GPa), Young's modulus Y (in unit GPa), Pugh's ratio B/G, Poisson's ratio ν, machinability index μ_{m}, and Vickers hardness H_{V} of $SrBO_3$ at different pressures.

Pressure/GPa	Compound	B	G	Y	B/G	ν	μ_{m}	H_{V}	Reference
0	$SrCrO_3$	170.97	84.45	217.54	2.02	0.28	1.49	12.46	this work
5		184.91	93.87	240.87	1.96	0.28	1.52	13.79	
10		208.36	102.48	264.14	2.03	0.28	1.64	15.13	
15		231.63	110.71	286.50	2.09	0.29	1.75	15.54	
20		247.83	118.52	306.68	2.09	0.29	1.80	16.64	
0		181.73	–	–	–	–	–	–	Ref. [46]
0	$SrFeO_3$	148.41	28.54	80.47	5.20	0.40	1.36	1.91	this work
5		175.96	39.75	110.91	4.42	0.39	1.57	2.92	
10		195.54	51.59	142.27	3.79	0.37	1.61	4.50	
15		216.12	61.69	169.00	3.50	0.36	1.68	5.79	
20		241.87	70.07	191.71	3.45	0.36	1.83	6.57	

The machinability index, μ_{m}, is increasingly significant for today's industrial applications because it determines a material's cutting force, optimum economic level of machine use, and plastic strain. This index (μ_{m}) is related to the machinability of a material by[64]

$$\mu_{\mathrm{m}} = \frac{B}{C_{44}}. \tag{4}$$

We find that the μ_{m} values increase as pressure rises (Table 3). Moreover, B is closely related to μ_{m}, and the result of μ_{m} also confirms the influence of pressure on the studied systems. This parameter is also significant for measuring the plasticity and lubricating quality of a solid.[65–67] Our studied systems reveal a higher value of μ_{m} under all pressure conditions than those of other materials,[55,68] indicating excellent lubricating properties and a lower friction value, which may have potential applications in today's industry.

3.3. Electronic properties

3.3.1. Band structure and density of states

Electronic band structure calculations are one of the most significant features of crystalline solids, as they almost completely determine the charge transport and optical characteristics of materials. The band structure exhibits how the energy (E) of the allowed electronic states changes with momentum ($\hbar k$) in the reciprocal lattice space. These $E(k)$ plots within the Brillouin zone are also known as electronic dispersion curves. The features of electronic band structures under different pressures follow the same trend, therefore, only the band structures at 0 GPa and 20 GPa for both $SrCrO_3$ and $SrFeO_3$ are presented in Fig. 2, where the horizontal dashed line refers to the Fermi level E_{F}. The blue and red solid lines represent energy bands for up-spin and down-spin electrons, respectively. In the case of $SrCrO_3$ (Fig. 2(a)), it is observed that several valence and conduction bands cross the E_{F} along the X–R direction and overlap with each other for the up-spin state, implying no band gap, which demonstrates the metallic behavior. However, no band-crossing trend is noticed for the down-spin state; its wide band gap suggests semiconducting behavior. Hence, our calculations clarify that the $SrCrO_3$ is a perfect half-metal, similar to the perovskite $BaUO_3$,[43] even under pressure. Furthermore, it is clear that some of the conduction and valence bands slightly lift up and down respectively with pressure increasing from 0 GPa to 20 GPa as the gap between valence band maximum and conduction band minimum becomes slightly lower. This is a signature of the effect of pressureon $SrCrO_3$ in this study. Some other minor changes are not mentioned here. On the other hand, at 0-GPa pressure, $SrFeO_3$ (Fig. 2(b)) is also a half-metal like $SrCrO_3$, though the gap between valence band maximum and conduction band minimum for the down-spin state is very narrow. Under the applied pressure, some bands for the down-spin state cross the E_{F} along the X–R and $M\Gamma$ directions, showing metallic behavior for both spin states. This result demonstrates the prominent effect of pressure.

To explore the matter in greater depth, we display the total

density of states (TDOS) and partial density of states (PDOS) of SrBO_3 at 0-GPa and 20-GPa pressures, as well as the atomic contributions of various orbitals around E_F (Fig. 3). For theup-spin of $SrCrO_3$, the contribution of TDOS near E_F comes from Cr-3d and O-2p states (Fig. 3(a)). Asignificant overlap in energy between these orbitals implies hybridization and tendency toward the generation of covalent bonding. These two electronic states also contribute strongly to the formation of the valence bands (VBs) from −6.3 (for 0 GPa) and −6.9 (for 20 GPa) to E_F, making the compound metallic. However, for down-spin, these two states are affected by the conduction band, generating a band gap of 2.12 eV at 0 GPa and 1.93 eV at 20-GPa pressure. The variation of the band gap occurs due to the pressure effect. However, there are two intense peaks in the VB located at around −2 eV to −5 eV, due mainly to O-2p, which may be supposed to play an essential role in ascertaining the optical properties of $SrCrO_3$. Figure 3(b) illustrates the PDOS and TDOS feature of $SrFeO_3$. At zero pressure, the contribution of TDOS near E_F comes from the Fe-3d and O-2p electronic states, making the compound metallic for up-spin and semiconducting for down-spin, with a narrow band gap of 0.21 eV which is clearly seen in the band structure (Fig. 2(b)). Under the pressure of 20 GPa, the up-spin configuration remains the same. However, in the case of the down-spin configuration, Fe-3d is pulled by the valence band. Hence, the perovskite $SrFeO_3$ also becomes metallic for both spin states. Two large peaks of TDOS are found in a range from around −2 eV to −6 eV in the VB due to Fe-3d, and O-2p may also be responsible for the optical properties of $SrFeO_3$, similar to those of$SrCrO_3$.

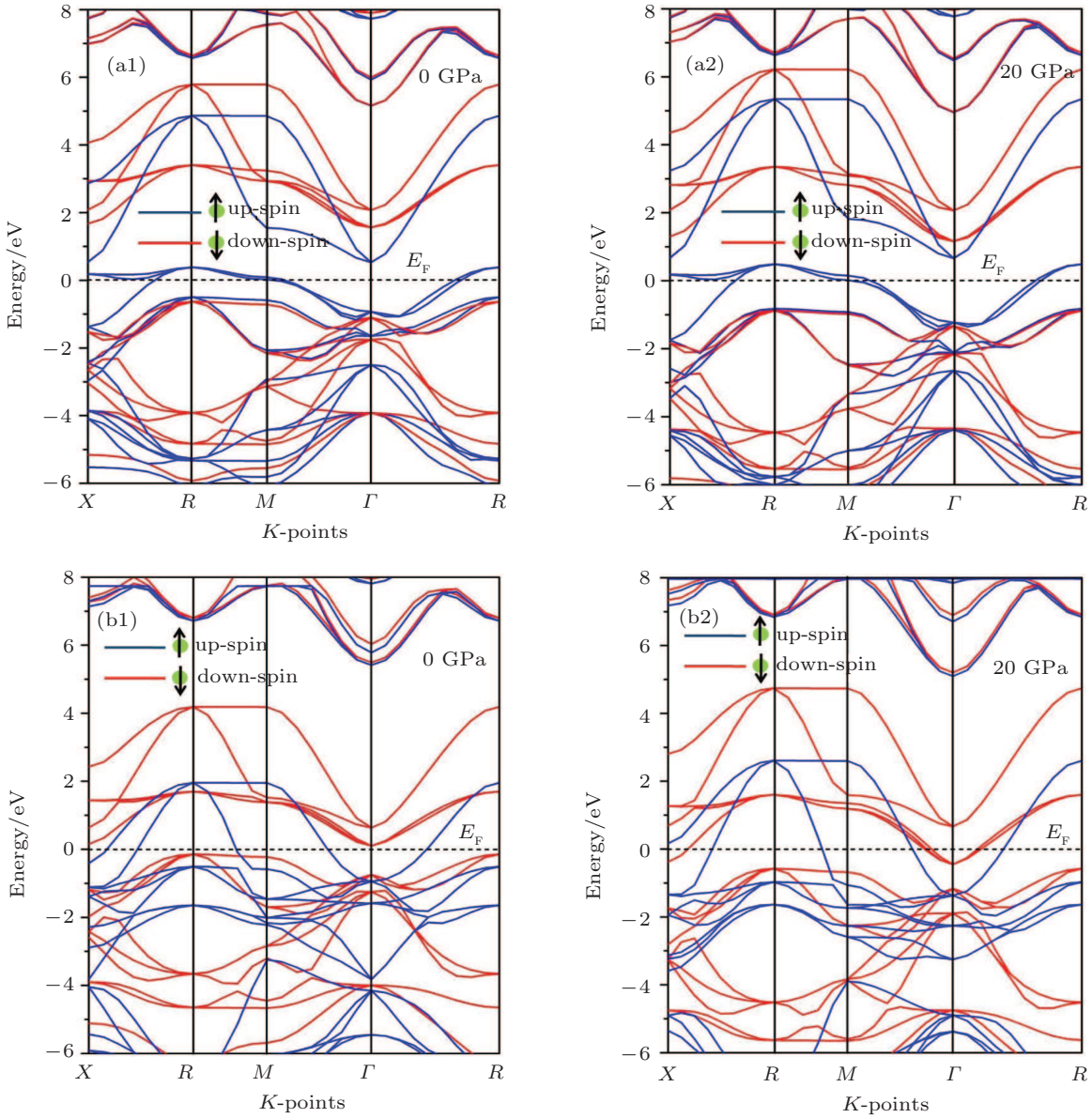


Fig. 2. Electronic band diagrams of [(a1) and (a2)] $SrCrO_3$ and [(b1) and (b2)] $SrFeO_3$ at 0-GPa and 20-GPa pressures.

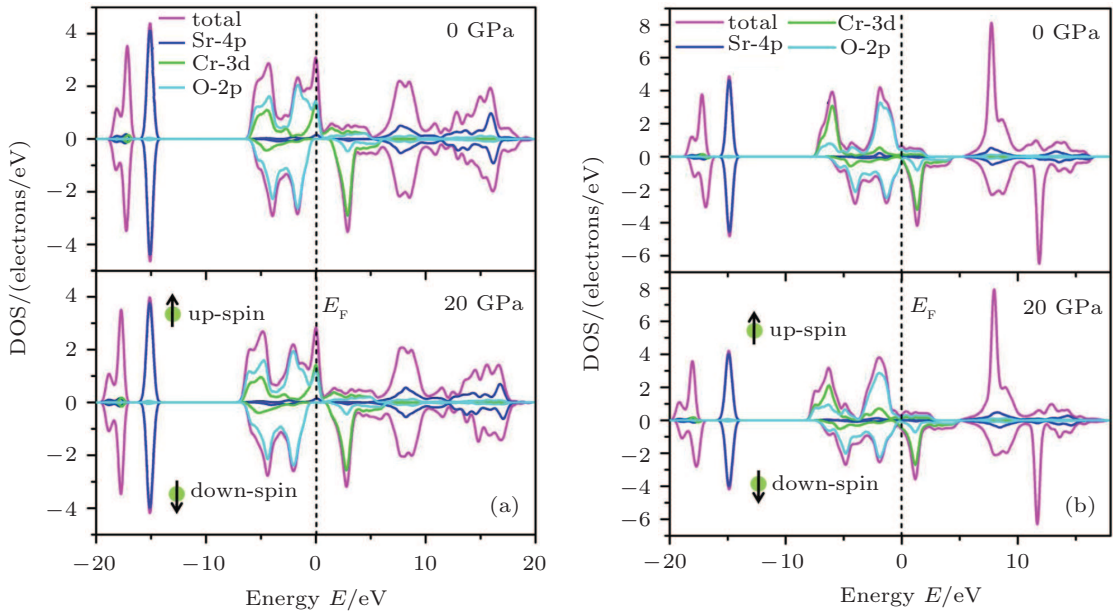


Fig. 3. PDOS and TDOS model of (a) $SrCrO_3$ and (b) $SrFeO_3$ at 0-GPa and 20-GPa pressures.

3.3.2. Electronic charge density

The charge density (in units of e/Å^3) maps under pressures of 0 GPa and 20 GPa are presented in Fig. 4 to elucidate the bonding nature in SrBO$_3$ materials. The scale on the right of Figs. 4(a) and 4(b) are used to show the intensities of charge density where blue and red represent low and high intensity, respectively.

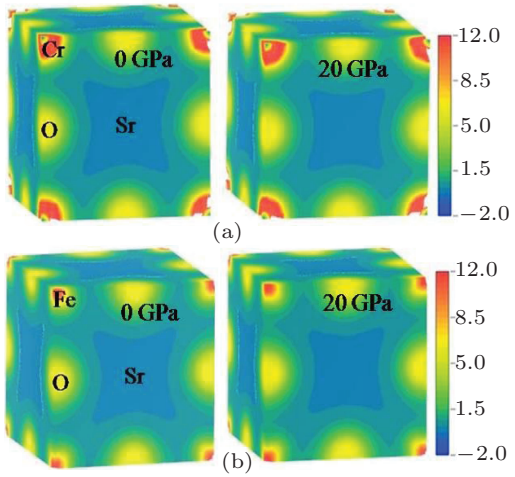


Fig. 4. Charge density mapping of (a) $SrCrO_3$ and (b) $SrFeO_3$ at 0-GPa and 20-GPa pressures.

The Cr–O bond in $SrCrO_3$ coincides with the hybridization between Cr-3d and O-2p orbital in TDOS (Fig. 3(a)), while the Fe–O bond in $SrFeO_3$ coincides with the hybridization between Fe-3d and O-2p orbitals in TDOS (Fig. 3(b)). The formation of charge density is not perfectly spherical in the surrounding region of all atoms, especially around Cr and Fe atom, showing the covalent nature of Cr–O and Fe–O bonds in $SrBO_3$. Though the change in bonding property is not so visually apparent, there is a slight decrease in Cr–O and Fe–O bond lengths with pressure increasing (Table 4), which may affect the bonding strength.

3.4. Optical properties

The study of optical properties is an effective way to determine the characteristics of a material subjected to incident electromagnetic waves. Measuring the behavior of various optical parameters at different spectral frequencies or energy values is also necessary to grope for the feasible optoelectronic and photovoltaic device applications of the compounds of interest. In this regard, the optical response of a compound to infrared, visible, and ultraviolet spectrum is extremely relevant. We investigate several energy(frequency)-dependent optical constants, to examine the response of SrBO$_3$ to the incident photons with different energy values: the real part of dielectric constant ε, the real part of refractive index n, the absorption coefficient α, optical conductivity σ, reflectivity R, and loss function L (Fig. 5).

Figure 5(a) exhibits the dielectric constants (ε). The peaks of ε are related to electron excitement that originates predominantly from intraband transitions and displays minor peaks between 0 eV–10 eV for both compounds under pressure. In the case of metallic materials, the spectra in the low energy infrared regions come from the intraband contributions of conduction band electrons. The SrBO$_3$ perovskites show a metallic characteristic that is very clear from their band structures. Therefore, the conduction electrons exhibit these intraband transitions. The dielectric values are high in the low-

frequency region and start to fall with the increase in energy of the incident photon. This characteristic of the dielectric curve is important for microelectronic applications and the large-scale integration of integrated circuits.[69,70] At 20-GPa pressure, ε initially decreases to some extent. Figure 5(b) illustrates the refractive indices (n) of $SrCrO_3$ and $SrFeO_3$. The real part of the refractive index discribes the phase velocity of propagation of the electromagnetic wave in the material. The maximum n is found to be due to the transition of electrons from the valence band to the conduction band. The maximum value of n ($\sim$ 5 and 4.2 for $SrCrO_3$ and $SrFeO_3$, respectively, at 0 GPa) is obtained at zero photon energy, which suggests that the studied materials have potential applications in devices such as QLEDs, OLEDs, solar cells, and waveguides.[68,71] We also observed a clear pressure effect, as the refractive index decreases to 3.6 and 3.8 for $SrCrO_3$ and $SrFeO_3$, respectively, at 20 GPa. Figure 5(c) shows the absorption spectra (α) of $SrBO_3$. Moreover, α describes the conversion of optimal photon energy (solar energy) into the efficiency of a material. This may occur due to the free electrons within the conduction band of material and offers the knowledge of the light-harvesting capability of a material, which can explain the efficiency of solar cells as a function of incident energy. The absorption coefficient is quite high in an energy range of $\sim$ 23 eV–25 eV for both perovskites, even under pressure, which ensures their potential application in solar panels. Figure 5(d) shows the optical conductivity (σ) of $SrCrO_3$ and $SrFeO_3$. This results in increasing the number of electrons in the conduction band and holes within the valence band. The σ starts with zero energy, suggesting no band gap, once again confirming the metallic nature of our compounds. The electrical conductivity (photoconductivity) values of the materials increase with photon energy increasing, and the spectra attain their maximum values at $\sim$24 eV. Therefore, the materials are expected to be electrically conductive, which ensures the conventional application sides of these compounds. Figure 5(e) displays the reflectivity (R) spectra of the compounds under consideration. It is seen that at 0 GPa, both $SrCrO_3$ and $SrFeO_3$ exhibit 50% and 42% reflectivities of total radiation at zero photon energy with a few peaks in the area of high-energy region due to the interband contributions. At 20 GPa, we observed 36% and 38% reflectivities for $SrCrO_3$ and $SrFeO_3$, respectively. We also observe that the reflectivity is interestingly low in the IR-visible region, which implies that if these materials are used in the solar panel, they will allow the visible spectra necessary for producing a photocurrent. This, in turn, will greatly increase the efficiency of solar panels. In addition, the high value of R ($\sim$64% and 58% for $SrCrO_3$ and $SrFeO_3$, respectively) at $\sim$25 eV proves their potential applications in serving as superior coating elements for minimizing solar heating. Figure 5(f) reveals the loss function (L) of $SrCrO_3$ and $SrFeO_3$. This particular optical parameter shows how a fast charged particle loses energy via exciting plasmon modes as it passes through the compound. We see a strong plasma peak around $\sim$27 eV at 0 GPa and a slight deviation at 20 GPa for both compounds under study, corresponding to their plasma frequency ω_p. It is interesting that at the plasma frequency, absorption, conductivity, and reflectivity fall sharply. The studied material will become transparent and will switch from metallic to insulating properties when the frequency corresponding to incident photon energy is higher than the plasma frequency.

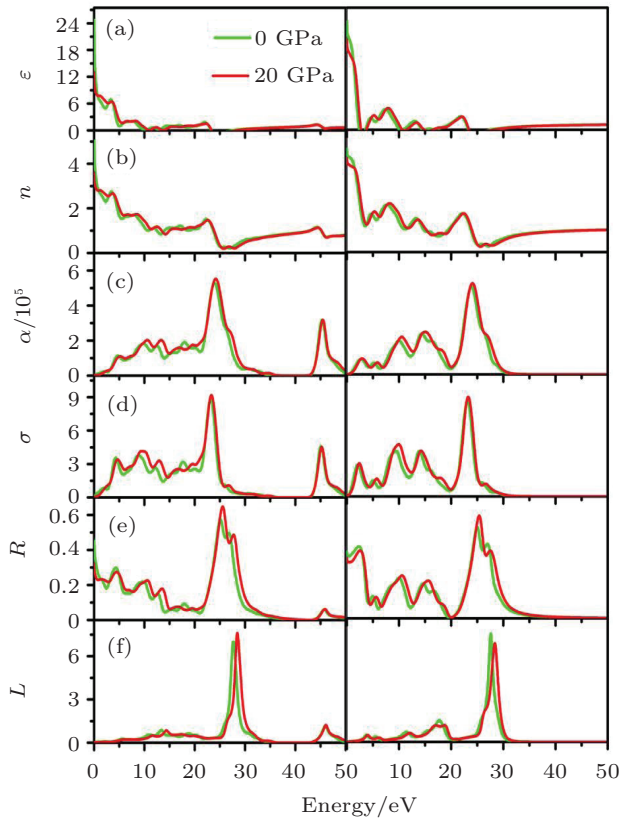


Fig. 5. Energy-dependent dielectric function (real part, ε), refractive index n, absorption coefficient α, conductivity σ, reflectivity R, and loss function L of $SrCrO_3$ (left side) and $SrFeO_3$ (right side).

3.5. Population analysis

Mulliken atomic population analysis provides many interesting results about the behaviors of bonding inside the materials.[72] The calculated information about population analysis for $SrBO_3$is shown in Table 4 at different pressures. Table 4 shows the positive values of the overlap population, which are higher than zero for both perovskites in this study, revealing that their covalent nature which nicely satisfies the result of charge density mapping (Fig. 4). Interestingly, the bonding between Cr and O (Cr–O) in $SrCrO_3$ is more covalent at different hydrostatic pressures (0 GPa–20 GPa) than

the bonding between Fe and O (Fe–O) in $SrFeO_3$. Under the application of pressure, the Cr–O and Fe–O bond lengths in $SrBO_3$ slightly decrease, which means that bond strengths slightly increase in both perovskites.

Table 4. Calculated Mulliken bond number n^{μ}, bond length d^{μ}, and bond overlap population P^{μ} of $SrCrO_3$ and $SrFeO_3$ compounds.

Pressure/GPa	Compound	Bonds	n^{μ}	d^{μ}/Å	P^{μ}
0	$SrCrO_3$	Cr–O	3	1.92485	1.25
5		Cr–O	3	1.90694	1.28
10		Cr–O	3	1.89111	1.29
15		Cr–O	3	1.87686	1.31
20		Cr–O	3	1.86406	1.33
0	$SrFeO_3$	Fe–O	3	1.91718	0.96
5		Fe–O	3	1.89784	0.99
10		Fe–O	3	1.88100	1.01
15		Fe–O	3	1.86602	1.04
20		Fe–O	3	1.85249	1.06

4. Conclusions

In this study, we provided a comprehensive explanation of the physical properties of $SrBO_3$ perovskites under pressure. The lattice parameters show a decreasing trend with applied pressure rising, and the mechanical stability is confirmed by the materials' elastic constants. The Poisson's ratio and Pugh's ratio reveal the ductility of pressure-dependent perovskite systems. The calculated hardness of $SrCrO_3$ is higher than that of $SrFeO_3$ under all applied pressures. The calculated band structures and DOS demonstrate the materials' half-metallic/metallic nature. The study of charge density and bond overlap population exhibits covalent bonding inside each compound. We also investigated the pressure-dependent optical properties of $SrBO_3$, exhibiting their potentials for several interesting applications such as in microelectronics, ultra-large-scale integration of integrated circuits, QLEDs, OLEDs, solar cells, waveguides, and solar heating reduction.

References

[1] Macchesney J B, Jetzt J J, Potter J F, Williams H J and Sherwood R C 1966 *J. Am. Ceram. Soc.* **49** 644
[2] Fu W T, Visser D, Knight K S and Ijdo D J W 52004 *J. Solid State Chem.* **177** 166
[3] Lines M E and Glass A M 1977 *Principles and Applications of Ferroelectrics and Related Materials* (Oxford: Clarendon Press)
[4] Banach G and Temmerman W M 2004 *Phys. Rev. B* **69** 054427
[5] Jaya S M, Jagadish R, Rao R S and Asokamani R 1991 *Phys. Rev. B* **43** 13274
[6] Mattheiss L F 1972 *Phys. Rev. B* **5** 290
[7] Shinjo T, Hosoito N, Takada T, Takano M and Takeda Y 1980 FERRITES: *Proceedings of The International Conference* 393
[8] Hodges J P, Short S, Jorgensen J D, Xiong X, Dabrowski B, Mini S M and Kimball C W 2000 *J. Solid State Chem.* **151** 190
[9] Kawasaki S, Takano M and Takeda Y 1998 *Solid State Ionics* **108** 221
[10] Murtaza G, Ahmad I, Amin B, Afaq A, Maqbool M, Maqssod J, Khan I and Zahid M 2011 *Opt. Mater.* **33** 553
[11] Kemmler-Sack S and Hofelich I 1971 *Z. Naturforsch* **26b** 539
[12] Ali Z, Ahmad I, Khan I and Amin B 2012 *Intermetallics* **31** 287
[13] Rao C N R and Raveau B (eds.) 1998 *Colossal Magnetoresistance, Charge Ordering and Related Properties of Manganese Oxides* (Singapore: World Scientific)
[14] Tokura Y (ed.) 2000 *Colossal Magnetoresitive Oxides* (New York: Gordon and Breach)
[15] Soderholm L, Skanthakumar S, Staub U, Antonio M R and Williams C W 1997 *J. Alloys Compd.* **250** 623
[16] Ali Z and Ahmad I 2013 *J. Electron. Mater.* **42** 438
[17] Ali Z, Khan I, Ahmad I, Naeem S, Rahnamaye Aliabad H A, Asadabadi S J and Zhang D 2013 *Physica B* **423** 16
[18] Mete E, Shaltaf R and Elliatroglu S 2003 *Phys. Rev. B* **68** 035119
[19] Kriener M, Braden M, Sneff D, Zabara O and Lorenz T 2007 *J. Magn. Magn. Mater.* **310** e187
[20] Michel C R, Sago A S, Guzman-Colin H, Lopes-Mena E R, Lardizabal D and Buassi-Monroy O S 2004 *Mater. Res. Bull.* **39** 2295
[21] Henrich V E and Cox P A 1966 *The Surface Science of Metal Oxides* (Cambridge: Cambridge University Press)
[22] Lan Y C, Chen X L and He M 2003 *J. Alloys Compd.* **354** 95
[23] Nekrosov I A, Held K, Keller G *et al.* 2006 *Phys. Rev. B* **73** 155112
[24] Belik A A, Azuma M, Saito T, Shimakawa Y and Takano M 2005 *Chem. Mater.* **17** 269
[25] Fang Z, Takahashi N, Asamitsu A, Mathieu R and Ogasawara T 2003 *Science* **302** 92
[26] Ortega-San-Martin L, Williams A J, Rodgers J, Attfield J P, Heymann G and Huppertz H 2007 *Phys. Rev. Lett.* **99** 255701
[27] Akhtar M J and Khan R T A 2011 *Materials Characterization* **62** 1016
[28] Zhou J S, Jin C Q, Long Y W, Yang L X and Goodenough J B 2006 *Phys. Rev. Lett.* **96** 046408
[29] Chamberl and B L 1967 *Solid State Commun.* **5** 663
[30] Williams A J, Gillies A, Attfield J P, Heymann G, Huppertz H, Martinez-Lopez M J and Alonso J 2006 *Phys. Rev. B* **73** 104409
[31] Long Y W, Yang L X, Zhou J S, Jin C Q and Goodenough J B 2006 *Phys. Rev. Lett.* **96** 046408
[32] Castillo-Martinez E and Alario-Franco M A 2007 *Solid State Sci.* **9** 564
[33] Jaya S M, Jagadish R, Rao R S and Asokamani R 1992 *Mod. Phys. Lett. B* **6** 103
[34] Takeda T, Yamaguchi Y and Watanabe H 1972 *J. Phys. Soc. Jpn.* **33** 967
[35] Nasu S 2000 *Focused on Frontiers of Magnetism Studies with Microscopic Proverbs*, Riken Review No. 27
[36] Kawasaki S, Takano M and Takeda Y 1996 *J. Solid State Chem. A* **121** 174
[37] Kawasaki S, Takano M and Takeda Y 1998 *Solid State Ionics* **108** 221
[38] Mac Chesney J B, Sherwood R C and Potter J F J 1965 *Chem. Phys.* **43** 1907
[39] Morimoto S, Yamanaka T and Tanaka M 1997 *Physica B* **237–238** 66
[40] Kawakami T and Nasu S 2005 *J. Phys.: Condens. Matter* **17** S789
[41] Tariq S, Jamil M I, Sharif A, Ramay S M, Ahmad H, Qamar N and Tahir B 2018 *Appl. Phys. A* **124** 43
[42] Somia, Mehmood S, Ali Z, Khan I, Khan F and Ahmad I 2019 *J. Electron. Mater.* **48** 1730
[43] Ali Z, Ahmad I and Reshak A H 2013 *Physica B* **410** 217
[44] Feng L, Liu Z and Liu Q 2012 *Physica B* **407** 2009
[45] Zhu Z L, Gu J H, Jia Y and Hu X 2012 *Physica B* **407** 1990
[46] Noor N A, Saddique M B, Haq B U, Laref A and Rashid M 2018 *Phys. Lett. A* **382** 3095
[47] Mehmood S, Ali Z, Khan I and Ahmad I 2017 *Mater. Chem. Phys.* **196** 222
[48] Mehmood S, Ali Z, Khan I and Ahmad I 2020 *J. Electron. Mater.* **49** 3780
[49] Khon W and Shams L J 1965 *Phys. Rev.* **140** A1133
[50] Perdew J P, Burke K and Ernzerhof M 1996 *Phys. Rev. Lett.* **77** 3865
[51] Clark S J, Segall M D, Pickard C J, Hasnip P J, Probert M I J, Refson K and Payne M C 2005 *Zeitschrift Fur Krist.* **220** 567
[52] Vanderbilt D 1990 *Phys. Rev. B* **41** 7892
[53] Fischer T H and Almlof J 1992 *J. Phys. Chem.* **96** 9768
[54] Monkhorst H J and Pack J D 1976 *Phys. Rev. B* **13** 5188
[55] Majumder R and Hossain M M 2019 *Comput. Cond. Matter* **21** e00402
[56] Majumder R, Mitro S K and Bairagi B 2020 *J. Alloys Compd.* **836** 155395
[57] Murnaghan F D 1937 *Am. J. Math.* **59** 235
[58] Mouhat F and Coudert F X 2014 *Phys. Rev. B* **90** 224104

[59] Hill R 1952 *Proc. Soc. Lond. A* **65** 349

[60] Maibam J, Sharma B I, Bhattacharjee R, Thapa R K and Singh R B 2011 *Physica B* **406** 4041

[61] Frantsevich I N, Voronov F F and Bokuta S A 1983 *Elastic Constants and Elastic Moduli of Metals and Insulators Handbook* (Kiev: NaukovaDumka) p. 60

[62] Pugh S F 1954 *Philos. Mag.* **45** 823

[63] Mitro S K, Rahman M A, Parvin F and Islam A K M A 2019 *Int. J. Mod. Phys. B* **33** 1950189

[64] Sun Z, Music D, Ahuja R and Schneider J M 2005 *Phys. Rev. B* **71** 193402

[65] Vitos L, Korzhavyi P A and Johansson B 2003 *Nat. Mater.* **2** 25

[66] Puttlitz K J and Stalter K A 2004 *Handbook of lead-free solder technology for microelectronic assemblies* (New York: Springer, CRC Press) p. 98

[67] Phasha M J, Ngoepe P E, Chauke H R, Pettifor D G and Mann D N 2010 *Intermetallics* **18** 2083

[68] Rubel M H K, Hossain K M, Mitro S K, Rahaman M M, Hadi M A and Islam A K M A 2020 *Materials Today Commun.* **24** 100935

[69] Majumder R, Hossain M M and Shen D 2019 *Mod. Phys. Lett. B* **33** 1950378

[70] Majumder R, Sarker M A R, Hossain M M, Hossain M E, Shen D, Reza A K M S and Kabir M H 2019 *J. Sci. Res.* **11** 195

[71] Naher M I and Naqib S H 2020 *J. Alloys Compd.* **829** 154509

[72] Mulliken R S 1955 *J. Chem. Phys.* **23** 1841